



Brief Report

Arrays of TiO₂ Nanosphere Monolayers on GaN-Based LEDs for the Improvement of Light Extraction

Dohyun Kim ¹, Uijin Jung ¹, Wonjun Heo ², Navneet Kumar ¹ and Jinsub Park ^{1,2,*}¹ Department of Electronic Engineering, Hanyang University, Seoul 04763, Republic of Korea² Division of Nanosemiconductor Engineering, Hanyang University, Seoul 04763, Republic of Korea

* Correspondence: jinsubpark@hanyang.ac.kr; Tel.: +82-2-2220-2318

Abstract: We report on the fabrication of TiO₂ nanosphere (NS) monolayer arrays for the enhancement of light extraction quantum efficiency of GaN-based light-emitting diodes (LEDs). The fabricated TiO₂ NSs monolayer arrays were composed of different phases of anatase (An-) and amorphous (Am-) TiO₂. The arrays were transferred onto the topmost layer of LED chips via the facile icing transfer method. The LED chips covered with Am-TiO₂ NS monolayer arrays showed 3.0- times enhanced light output power intensity compared with reference LED chips at a fixed injection current of 100 mA. The enhanced light extraction of LED chips by an Am-TiO₂ NS monolayer can be attributed to a high transmittance (91.1%) in visible and increased light extraction probability of photons generated in LEDs, resulting from the enhanced light coupling efficiency by reduced total internal reflection (TIR). Finite-difference time-domain (FDTD) simulation results also agreed well with the experimentally observed results. Based on the experimental and theoretical results, our suggested Am- and An-TiO₂ NS arrays can be considered a very facile and effective method to improve the device performance of various visible LED chips.

Keywords: TiO₂ nanosphere monolayer; transfer method; GaN LED; light extraction; compound semiconductor



Citation: Kim, D.; Jung, U.; Heo, W.; Kumar, N.; Park, J. Arrays of TiO₂ Nanosphere Monolayers on GaN-Based LEDs for the Improvement of Light Extraction. *Appl. Sci.* **2023**, *13*, 3042. <https://doi.org/10.3390/app13053042>

Academic Editor: Carolina Belver

Received: 19 January 2023

Revised: 16 February 2023

Accepted: 24 February 2023

Published: 27 February 2023



Copyright: © 2023 by the authors. Licensee MDPI, Basel, Switzerland. This article is an open access article distributed under the terms and conditions of the Creative Commons Attribution (CC BY) license (<https://creativecommons.org/licenses/by/4.0/>).

1. Introduction

Titanium dioxide (TiO₂) has received a great deal of attention for its various applications in solar cells [1], gas sensors [2], photodetectors [3], lithium-ion batteries [4], and other optoelectronic devices [5] due to its superior properties such as chemical stability [6], high photocorrosion resistance [7], and non-toxicity [8]. Among the versatile applications of TiO₂ nanostructures for light generation and guiding, diverse surface morphologies such as nanoparticles [9], nanotubes [10], nanowires [11], submicron/nanospheres [12,13], and mesoporous structures [14] have been extensively investigated. For light extraction enhancement of GaN-based light emitting diodes (LEDs) to achieve high quantum efficiency, TiO₂ nanomaterials, including micro-pillars [15] and nanopatterns [16], have been especially suggested as potential candidates for light extractors that minimize the total internal reflection (TIR) due to their wide band gap (~3.5 eV at room temperature) [17], high transmittance (~90%) [18] in the visible region, and refractive indices ($n = 2.8$ for the anatase phase and $n = 2.5$ for the amorphous phase) intermediate to those of GaN and air [19].

Recently, the utilization of metal oxide nano- and microsphere-type nanostructures has been reported to augment the light extraction efficiency of LED chips [20,21]. Such nanostructures offer advantages such as the ease of formation of arrayed nano- and microspheres via a simple transfer method [22]. Previous reports used a poly vinyl alcohol (PVA) attaching layer to transfer the monolayer array. The use of PVA can, however, degrade the reliability and efficiency of the LED chips because thermal damage can occur with the long annealing process at high temperatures necessary for the removal of PVA [23]. Therefore, to universally use the transferrable metal oxide micro/nanosphere monolayer

without limiting the substrate material, the reduction of post-thermal annealing damage is an essential issue. Among the possible methods, the icing transfer method may be a good candidate because during processing, it uses deionized (DI) water as a binder with a soft baking temperature and short time (60 °C/ 30 s), none of which causes severely harmful effects, such as the deformation or degradation of the device.

In this study, we fabricated a uniformly arrayed TiO₂ NSs monolayer with different crystal structures of amorphous (Am-TiO₂) and anatase (An-TiO₂) and transferred them onto the LED chips to enhance the light extraction efficiency. The formation of the ordered TiO₂ NS monolayer array and its transfer were conducted by a simple unidirectional rubbing method and icing transfer method assisted by DI water. Our transferrable TiO₂ NS monolayer arrays can be an excellent way to improve the device performance of LED chips. The experimental and finite-difference time-domain (FDTD) simulation-based theoretical results confirmed that the Am-TiO₂ NSs monolayer enhanced the extraction efficiency of LED chips.

2. Materials and Methods

For the fast synthesis of TiO₂ NSs, we used a solution process method. First, we mixed acetonitrile 40 mL, ethanol 50 mL, methylamine and H₂O solvents with magnetic stirring (Solution A). Ethanol 10 mL and titanium isopropoxide (TTIP) solvents were mixed with magnetic stirring (Solution B). Solutions A and B were mixed together in a 250 mL round bottom flask at room temperature for 1 h. TiO₂ NSs were collected by centrifugation and washed with DI water. TiO₂ NSs were then dried in an oven at 80 °C. The obtained as-synthesized amorphous TiO₂ (Am-TiO₂) NSs were converted to anatase TiO₂ (An-TiO₂) NSs through thermal treatment at 450 °C for 4 h.

Structural properties of the synthesized amorphous TiO₂ (Am-TiO₂) and anatase TiO₂ (An-TiO₂) NSs were investigated by scanning electron microscopy (SEM) (S-4800, Hitachi, Tokyo, Japan), and a high-resolution X-ray diffraction (HR-XRD) system (SmartLab, Rigaku, Tokyo, Japan) equipped with Cu-K α radiation (1.54 Å). Optical properties of the TiO₂ monolayers were analyzed by ultraviolet–visible light (UV-vis) spectroscopy (Lambda 650S, Perkin Elmer, Waltham, MA, USA). To evaluate the light extraction and electrical properties of the LED chips with TiO₂ NSs monolayers, light output power–current–voltage (L–I–V) measurements were conducted (Keithley 2400, Tektronix, Beaverton, OR, USA).

GaN-based LED epi-structures were grown on a c-plane sapphire substrate via metal–organic chemical vapor deposition (MOCVD). Trimethylgallium (TMGa), trimethylindium (TMIn) and NH₃ were used as the Ga, In, and N precursors, respectively. The LED structures consisted of a 1 μ m thick unintentionally doped GaN layer, a 2 μ m thick n-type GaN layer, six pairs on an InGaN/GaN multiple quantum well (MQWs) active layer, and a 0.3 μ m thick p-type layer. The active layer consisted of six pairs, each with a 3 nm thick InGaN well layer and a 10 nm thick GaN barrier layer in the MQWs [24]. To fabricate the chip, blue LED wafers were partially etched by inductively coupled plasma (ICP) until the n-type GaN layer was exposed. Indium tin oxide (ITO, 100 nm) was evaporated to the surface of p-GaN for current spreading. Cr/Au electrodes (10/500 nm) were subsequently evaporated as both n- and p-type electrodes for contact metal. Finally, LED wafers were divided into chips with an area of 600 \times 600 μ m².

3. Results

3.1. Transfer of TiO₂ Nanosphere Monolayer onto GaN-LEDs

To form the TiO₂ NS monolayer array, TiO₂ NSs were formed on a PDMS pad with the elegant unidirectional rubbing method described in other references [25] and as shown in Figure 1a. Then, DI water was drop-cast on the surface of the LED chips, and a flipped TiO₂/PDMS pad was placed on them (Figure 1b). After freezing the DI water for 10 min under –18 °C conditions, the PDMS pad was peeled from the LED chip (Figure 1c). The TiO₂ NS structure left behind formed monolayer arrays on the LED chips, as displayed in Figure 1d.

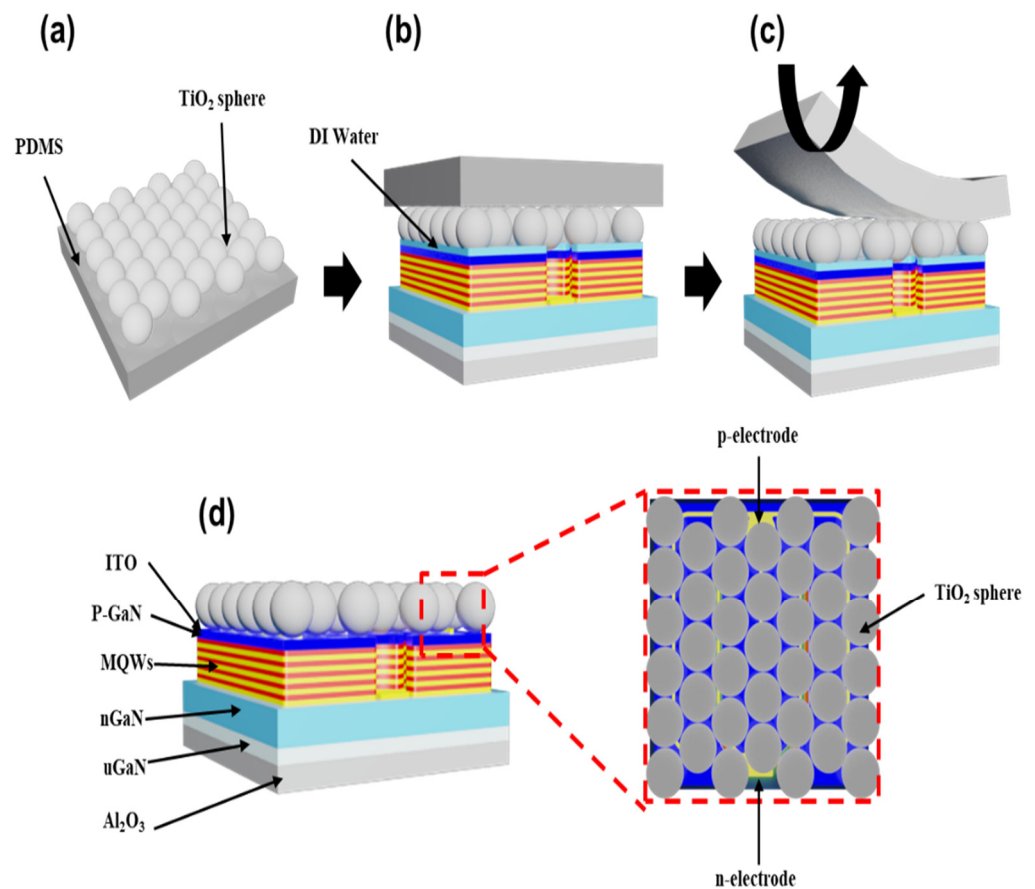


Figure 1. Process flow from formation of TiO₂ monolayer to its transfer on LED chips. (a) Formation of TiO₂ NSs ML on a PDMS, (b) drop-casting of DI water and flip of TiO₂/PDMS pad, (c) removing of PDMS from TiO₂ NSs ML, (d) formation of arrays of TiO₂ NSs ML on LED chips.

3.2. Structural and Optical Characterization of TiO₂ Nanospheres

The surface morphologies of Am- and An-TiO₂ NSs synthesized by solution-based synthesis method are observed by SEM as shown in Figure 2a,b, respectively. Figure 2a,b shows the uniformly distributed sizes and morphologies of as-synthesized and calcinated TiO₂ NSs. The average diameters of Am- and An-TiO₂ NSs were measured as 498 ± 5 nm and 496 ± 5 nm, respectively, as depicted in the inset of Figure 2. The summary of the size dependence of TiO₂ NSs with respect to the mixed solution ratio is depicted in Table S1. Generally, the solution-based synthesis of TiO₂ NSs is governed by a hydrolysis process [26]. Initially, the stepwise hydrolysis forms primary TiO₂ hydrates with sizes of a few nanometers, which have high surface energy and small electrostatic charges. Hence, TiO₂ hydrates agglomerate spontaneously owing to van der Waals attractive forces and hydrogen bonding among the individuals [27]. As the mass of the TiO₂ hydrates increases by gradual aggregation of the individual hydrates, the electrostatic charges build up in the aggregated TiO₂ hydrates. When TiO₂ spheres achieve a certain critical size, the repulsive interaction becomes sufficiently strong to block the Brownian aggregation, leading to each TiO₂ sphere being completely separate and without further increase in size.

To investigate the phase conversion of the TiO₂ spheres from as synthesized to after annealing at different temperatures, we analyzed the XRD patterns. Figure 3a shows the XRD spectra of the Am- and An-phase TiO₂ NSs drop-casted on the Al₂O₃ substrate. For the Am-TiO₂ NSs, there are no strong peaks in the XRD pattern, indicating that there is no crystallized phase, as shown (black line) in Figure 3a. By increasing the annealing conditions to 450 °C for 4 h, strong 2 θ peaks appeared at the diffraction peaks placed at 25.2°, 37.8°, 48°, 55°, 62.6°, 70.3°, and 75°, which are well matched with crystal planes (101), (103), (200), (105), (204), (220), and (215) of An-structured TiO₂ (JCPDS No. 21-1272), as

shown (red line) in Figure 3a. According to the XRD results, we know that as-synthesized Am-TiO₂ NSs changed to An-TiO₂ via heat treatment [28].

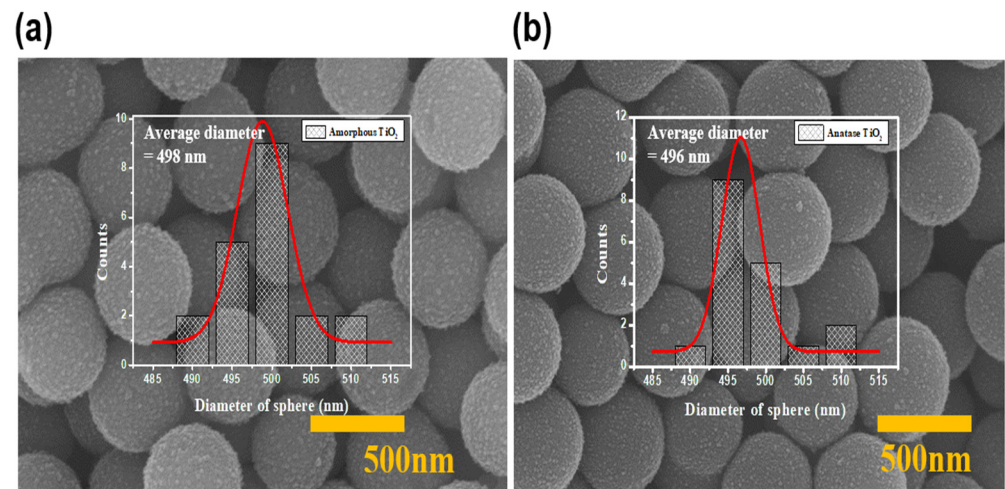


Figure 2. SEM images of (a) Am- and (b) An-TiO₂ NSs. The inset figure shows the size distributions of used TiO₂ NSs.

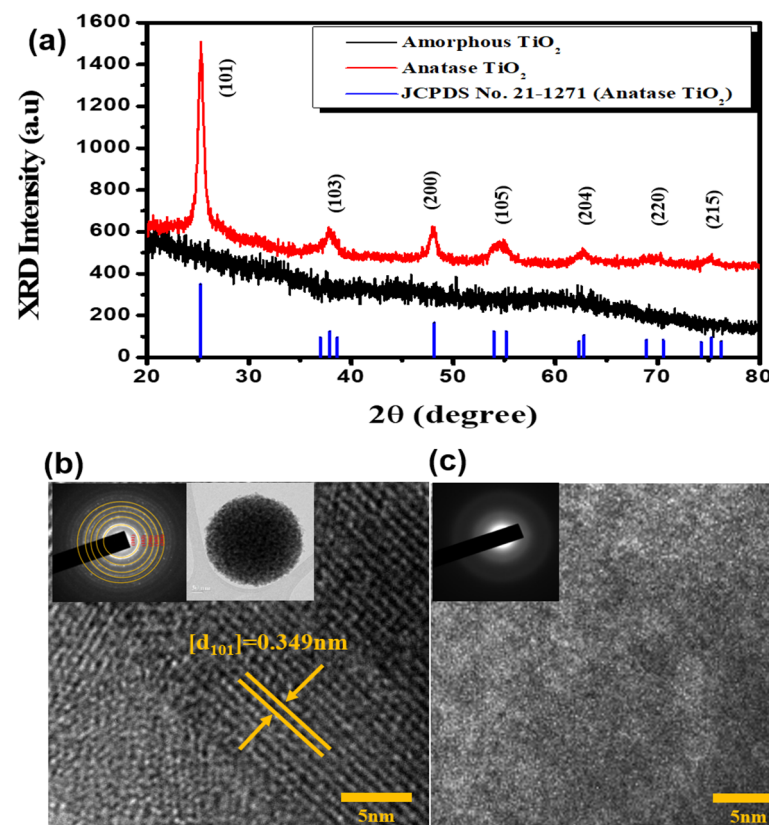


Figure 3. (a) XRD patterns of as-synthesized and thermally annealed TiO₂ NSs and HR-TEM images and SAED patterns of (b) anatase and (c) amorphous spheres.

Transmission electron microscopy (TEM) images further reveal that the Am- and An-TiO₂ NSs have clustered structures and consist of a number of tiny nanocrystals, as shown in Figure 3b,c. Figure 3b shows the TEM image of An-TiO₂ NSs with particle diameters of 496 ± 5 nm. The selected area electron diffraction (SAED) patterns of An-TiO₂ NSs show the crystallized An-TiO₂ NSs with indexing of (101), (103), (200), (105) and (204). The lattice-resolved HRTEM image clearly demonstrates that the crystal interplanar spacing

distance of (101) planes of An-TiO₂ is $d = 3.492 \text{ \AA}$ within the primary nanocrystals [29]. Am-TiO₂ NS, by contrast, does not present any diffraction pattern except for the blurry ring shape, as in XRD analysis, confirming the amorphous nature of this material.

To investigate the optical properties of the Am- and An-TiO₂ monolayers, the absorbance was measured using UV-vis spectroscopy. Figure 4a shows the absorbance spectra of the Am- (black line) and An- (red line) TiO₂ NSs monolayers. It clearly shows that the Am- and An-TiO₂ monolayers absorb only a range of UV light due to their wide band gap. We calculated the optical band gap of the used TiO₂ monolayers from a Tauc plot, as displayed in the inset image of Figure 4a, by a plot of the $(\alpha h\nu)^2$ versus $h\nu$ curves [30].

$$\alpha h\nu = A(h\nu - E_g)^m$$

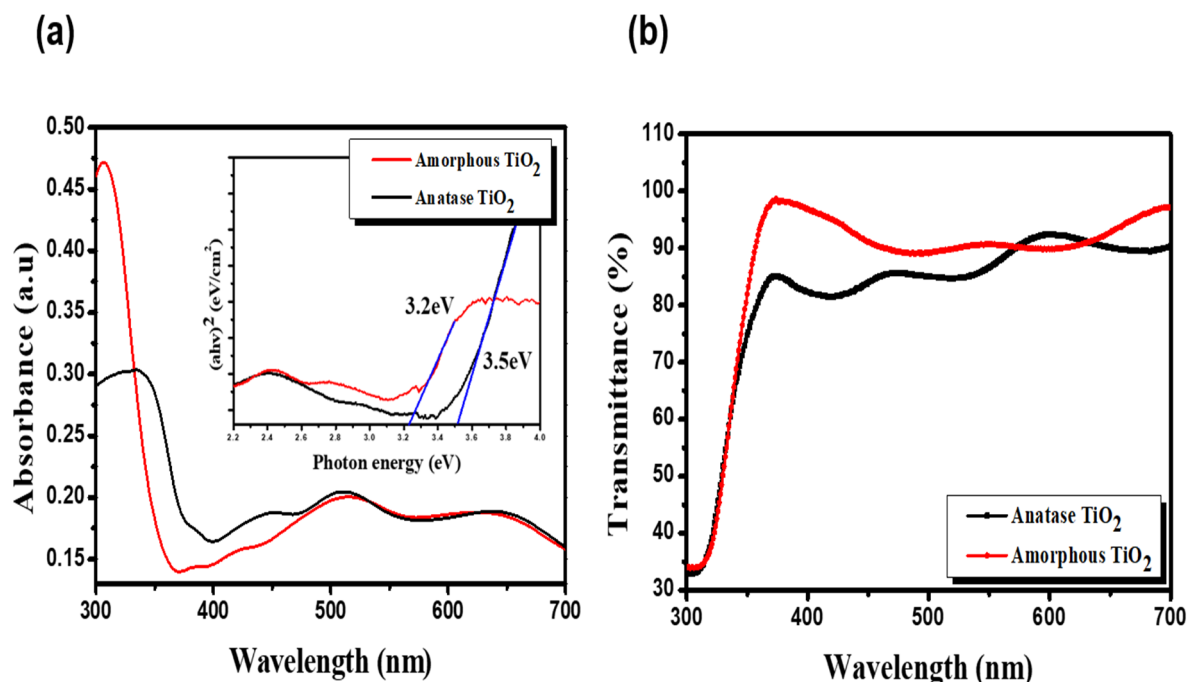


Figure 4. (a) Absorbance spectra and (b) transmittance of TiO₂ monolayers using An- (dot-line) and Am-TiO₂ (black-line) nanosphere monolayers.

Here, A is a constant, $h\nu$ is the incident photon energy, E_g is the optical band gap, α is an absorption coefficient, and the value of m is $1/2$ for indirect transitions. The calculated band gaps for the Am- and An-TiO₂ monolayers are about 3.5 eV and 3.2 eV, respectively. The bandgaps of fabricated TiO₂ monolayers are very similar to previously reported values [31].

In addition, Figure 4b shows the transmittance spectra of the Am-TiO₂ sphere and An-TiO₂ sphere monolayers. The transmittances of the Am-TiO₂ sphere and An-TiO₂ sphere monolayers were, respectively, 91.1 and 83.9% at a 450 nm wavelength. The high transmittance of TiO₂ spheres in the visible region resulting from their wide band gap and thickness of the monolayer indicates that TiO₂ NSs monolayers can be used as a light extractor in visible LEDs.

3.3. Effects of TiO₂ NS Monolayer on the Device Performance of LED

Following experimental methods, we fabricated TiO₂ NS arrays/LED chips. Figure S1a,b shows optical microscope images of a blue LED chip with Am- and An-TiO₂ NSs. The images clearly show that the TiO₂ NS monolayer was successfully formed and transferred on the fabricated LEDs chip via the icing transfer method. The magnified SEM images of Am- (Figure S1c,d) and An-TiO₂ (Figure S1e,f) NS arrays formed on p-GaN show the well-aligned sphere arrays of Am- and An-TiO₂ without surface damage.

The effects on the light extraction efficiency (LEE) of Am-TiO₂ and An-TiO₂ monolayers being transferred onto LED chips were investigated by optical and electrical performance measurements. The electroluminescence (EL) spectra for LED chips with Am- and An-TiO₂ monolayers were measured at the fixed injection current of 20 mA, as shown in Figure 5a. The effect on EL intensity of LED chips with Am-TiO₂ NS array is the strongest among the three samples. The integrated EL intensity of the samples covered with An-TiO₂ NS and Am-TiO₂ NS arrays exhibited enhancements of 1.3 and 7.9 times, respectively, over that of the reference LED chips at 443 nm emission wavelength. Optical microscopy images of emitted light obtained from LED chips with Am- and An-TiO₂ monolayer arrays are shown in the inset of Figure 5a.

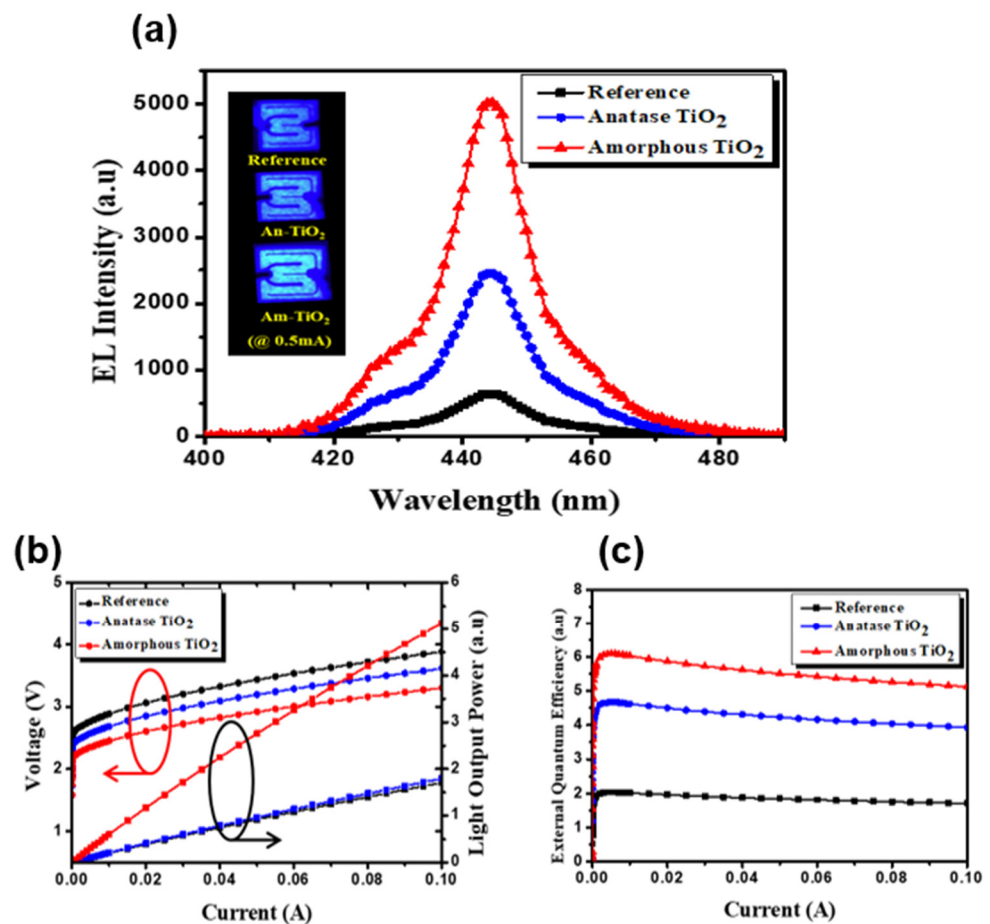


Figure 5. (a) EL spectra of LED chips with An- and Am-TiO₂ NS arrays with an injection current of 20 mA. Emission images of LED chips are shown in inset. (b) L-I-V curves and (c) external quantum efficiency (EQE) of LED chips with different TiO₂ NS arrays as a function of injected current (at $I = 0\sim 100$ mA).

LED chip with Am-TiO₂ monolayer arrays showed the brightest emission intensity and uniform emission area at a low current injection of 0.5 mA. These indicate that Am-TiO₂ NS monolayers can dramatically improve the light extraction of LED chips. In addition, to evaluate the LEE of the LED chips, light output powers (LOPs)–current–voltage (L-I-V) were measured at the injection current ranging from 0 to 100 mA, as shown in Figure 5b. The LOPs of the Am-TiO₂ NSs array/LEDs chip were higher by factors of 2.8 and 3.1 times compared to the An-TiO₂ monolayer-coated LED chip and reference LED chip, respectively, at 100 mA. This large enhancement in the LOP of LED chips with Am-TiO₂ NS arrays can be attributed to the efficient propagation of light from the GaN layer to the TiO₂ NS and superior mitigation of back reflection of light at the interface of TiO₂ NSs and air [32,33].

The external quantum efficiency (EQE) of the LED chips with and without a TiO₂ NS array at the injection current range of 0–100 mA were measured, as shown in Figure 5c. Although there are efficiency drops in data as current levels increase, LED chips with Am-TiO₂ NS arrays still showed higher EQE than other LED chips. EQE is expressed as $EQE = IQE \times LEE$, where IQE is the internal quantum efficiency and LEE is the light extraction efficiency. The values of IQE of all blue LED chips are assumed to be the same since they have the same epitaxial structure. Therefore, the improvement of the EQE of the LED chips with the Am-TiO₂ NS arrays results from the increased LEE of the LED chips at $I = 100$ mA. The measured EQE from the samples covered with An- and Am-TiO₂ NS arrays exhibited enhancements of 1.1 and 3.1 times more than a bare LED chip, respectively, at 100 mA. The EQEs of LEDs with Am-TiO₂ NS arrays exhibit a stable boost of 3 times over LEDs with An-TiO₂ NS arrays over the entire range of injection currents applied in this experiment. To design an adequate TiO₂ NS monolayer array on LEDs, various parameters should be considered, such as the refractive index, crystal structure, and the packing density of spheres. Among the considered parameters described here, we paid special attention to the effects of the crystal structure of the spheres on the LEE of LED chips. In order to theoretically evaluate LEEs of LEDs with respect to changes in the refractive indices of used spheres monolayers, which can be modified by changes in the crystal phases of TiO₂, we used the 3-D FDTD simulation method.

Figure 6a–c shows the far-field intensity mapping of the reference LED and LED chip with An- and Am-TiO₂ sphere monolayer arrays. It is apparent that emitted light was trapped in the inner LED chip due to TIR resulting from the abrupt change in the refractive index across p-GaN and air in the reference LED chip. However, the LED with An-TiO₂ monolayer arrays shows that light was effectively diffused from the LED chip through the An-TiO₂ NSs, as clearly shown in Figure 6b. Furthermore, the Am-TiO₂ monolayer array can more effectively diffuse a significant amount of light from the LED through the NSs, as depicted in Figure 6c. Similar to far-field intensity, Figure S2a–c shows the cross-section profiles of the power field for reference LED and LED chips with An- and Am-TiO₂ sphere monolayer arrays. It is clear from Figure S2a that emitted light was trapped in LEDs due to the abrupt change in the refractive index across p-GaN and air in the reference LED chips. However, the LEDs with An-TiO₂ and Am-TiO₂ NSs monolayer arrays demonstrate that light was effectively diffused from the LED chips through the NSs, as shown in Figure S2b and S2c, respectively. The enhancement of light extraction from LEDs with Am-TiO₂ NSs arrays can be attributed to the increase in the escape probability of photons from the LED as observed by simulation results. In addition, in terms of the escape angle of light, light emission of LED mainly occurred between 10° and 20° as denoted by the red dotted line in Figure 6a–c. The Am-TiO₂ monolayer array/LED shows the highest light-emission intensity and brightest area among all samples. In addition, by comparison of the integrated power field intensity for LEDs with different spheres of TiO₂ monolayers, LED chips with An-TiO₂ monolayers and Am-TiO₂ monolayer arrays exhibited, respectively, 1.4 times and 1.76 times higher intensity than LED chips without any structures.

To further investigate the increased light extraction via Am-TiO₂ NS monolayers as compared to An-TiO₂ NSs, we captured the evolution of traveling waves showing light propagation with respect to changes in time, as shown in Figure 7. When we compared the light extraction via different Am- and An-TiO₂ NSs, light propagation modes in Am-TiO₂ NSs were more strongly concentrated on the apex than were those of An-TiO₂ as denoted by yellow arrows in Figure 7j,d, respectively. The backscattering portions of light in An-TiO₂ spheres remaining from escaping via the top of TiO₂ spheres toward GaN are clearly larger than those of Am-TiO₂ as denoted by the red arrow in Figure 7f,l, respectively. Therefore, more photons can effectively escape from the apex of Am-TiO₂ NS concentrated by the convex lens-focusing effects and propagated via Am-TiO₂ NSs to air from the LEDs. This result further proved that the Am-TiO₂ NSs are more effective than An-TiO₂ NSs at improving the LEE of LEDs.

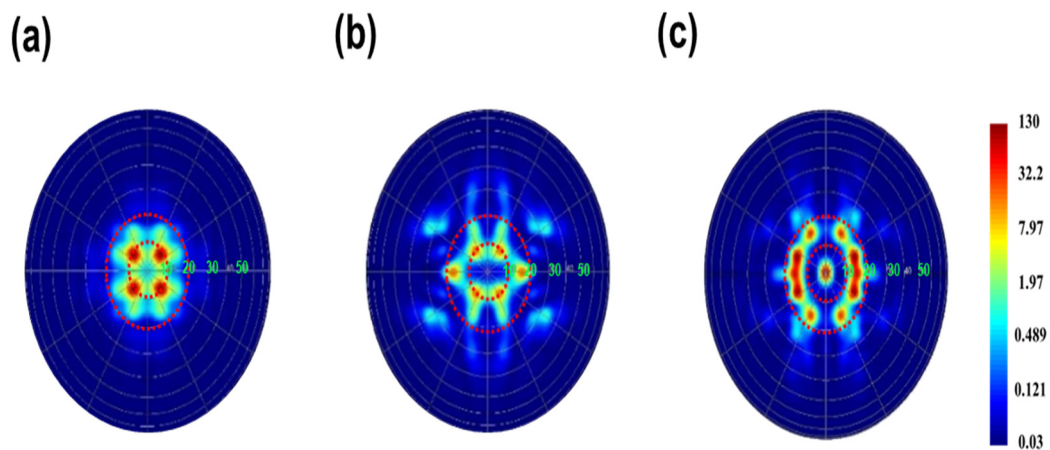


Figure 6. Far-field intensity mappings of (a) a reference LED and LEDs with (b) An-TiO₂ and (c) Am-TiO₂ NS monolayers.

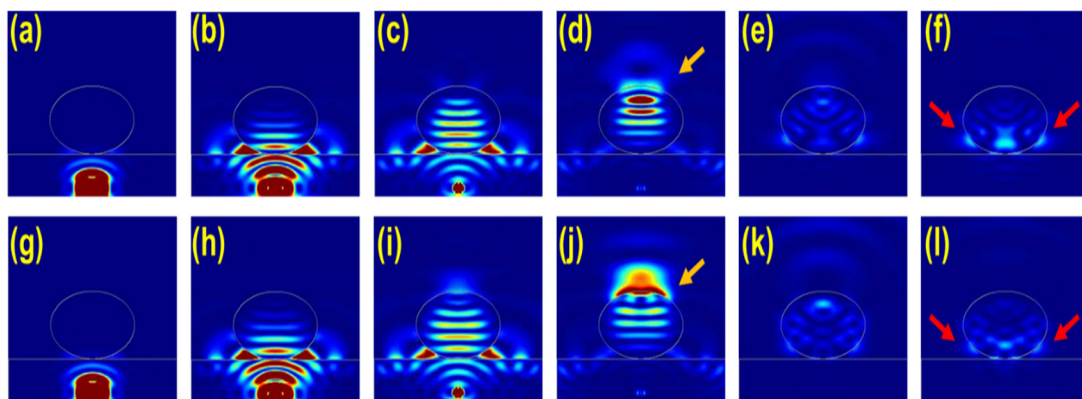


Figure 7. Evolution of travelling light via An-TiO₂ NSs (a–f) and Am-TiO₂ NSs (g–l) with respect to change of time. The red arrows represent the backscattering from the interface of air/TiO₂ sphere to p-GaN.

4. Conclusions

We successfully formed uniform monolayer arrays of TiO₂ NSs on LED chips via the icing transfer method. After the transfer of TiO₂ monolayers with different crystal phases onto LED chips, enhancements in the light extraction of LEDs were observed. The LEDs covered with Am- and An-TiO₂ NS monolayers showed 3.0- and 1.05-fold enhancement of LOP intensity, respectively, compared with the reference LEDs without the NSs at a fixed injection current of 100 mA. The experimentally measured results are entirely consistent with those of 3D-FDTD simulations, and the large enhancement in the optical output power can be attributed to the superior suppression of the TIR and backscattering between the GaN layer and air by Am-TiO₂ NS arrays and the concentration of light on the apex of spheres within light propagation path. Based on our results, the transferrable uniform arrays of Am- and An-TiO₂ NS monolayers will open a new path to improve the optical performance of various optoelectronic devices, such as solar cells, photodetectors, and LED chips.

Supplementary Materials: The following supporting information can be downloaded at: <https://www.mdpi.com/article/10.3390/app13053042/s1>, Figure S1: (a,b) Optical microscope image of the TiO₂ nanosphere arrays on blue LED chip with Am- and An-TiO₂ nanosphere. (c,d) and (e,f) show the SEM images of 500nm size Am- and An-TiO₂ nanosphere arrays on p-GaN substrate, respectively; Figure S2: (a–c) FDTD simulation results of compares cross sections of the power field for general planar LED and LEDs with Anatase-, Amorphous-TiO₂ sphere array (d,e) Anatase, Amorphous-

TiO₂ single sphere cross section image; Table S1: Summary of synthesized TiO₂ nanospheres sizes according to amount of the injected DIW.

Author Contributions: Conceptualization, J.P. and D.K.; methodology, D.K.; software, U.J.; validation, N.K. and D.K.; formal analysis, W.H.; investigation, D.K. and U.J.; writing—original draft preparation, D.K. and J.P.; writing—review and editing, N.K. and J.P.; supervision, J.P.; project administration, J.P.; funding acquisition, J.P. All authors have read and agreed to the published version of the manuscript.

Funding: This work was supported by the National Research Foundation of Korea(NRF) grant funded by the Korea government (MSIT) (No. 2021R1A4A1052085).

Conflicts of Interest: The authors declare no conflict of interest.

References

1. You, Y.; Tian, W.; Min, L.; Cao, F.; Deng, K.; Li, L. TiO₂/WO₃ Bilayer as Electron Transport Layer for Efficient Planar Perovskite Solar Cell with Efficiency Exceeding 20%. *Adv. Mater. Interfaces* **2020**, *7*, 1901406. [[CrossRef](#)]
2. Zhang, B.; Yang, F.; Liu, H.; Yan, L.; Yang, W.; Xu, C.; Huang, S.; Li, Q.; Bao, W.; Liu, B.; et al. Assembling Graphene-Encapsulated Pd/TiO₂ Nanosphere with Hierarchical Architecture for High-Performance Visible-Light-Assisted Methanol Electro-Oxidation Material. *Ind. Eng. Chem. Res.* **2019**, *58*, 19486–19494. [[CrossRef](#)]
3. Yang, T.; Park, S.J.; Kim, T.G.; Shin, D.S.; Park, J. Ultraviolet photodetector using pn junction formed by transferrable hollow n-TiO₂ nano-spheres monolayer. *Opt. Express* **2017**, *25*, 30843–30850. [[CrossRef](#)]
4. Zhu, K.; Li, Q.; Xue, Z.; Yu, Q.; Liu, X.; Shan, Z.; Liu, K. Mesoporous TiO₂ Spheres as Advanced Anodes for Low-Cost, Safe, and High-Areal-Capacity Lithium-Ion Full Batteries. *ACS Appl. Nano Mater.* **2020**, *3*, 1019–1027. [[CrossRef](#)]
5. Song, D.; Cui, P.; Wang, T.; Xie, B.; Jiang, Y.; Li, M.; Mbebgue, J.M. Bunchy TiO₂ hierarchical spheres with fast electron transport and large specific surface area for highly efficient dye-sensitized solar cells. *Nano Energy* **2016**, *23*, 122–128. [[CrossRef](#)]
6. Wu, F.; Zhou, Z.; Hicks, A.L. Life Cycle Impact of Titanium Dioxide Nanoparticle Synthesis through Physical, Chemical, and Biological Routes. *Environ. Sci. Technol.* **2019**, *53*, 4078–4087. [[CrossRef](#)] [[PubMed](#)]
7. Elseman, A.M.; Zaki, A.H.; Shalan, A.E.; Rashad, M.M.; Song, Q.L. TiO₂ Nanotubes: An Advanced Electron Transport Material for Enhancing the Efficiency and Stability of Perovskite Solar Cells. *Ind. Eng. Chem. Res.* **2020**, *59*, 18549–18557. [[CrossRef](#)]
8. Ton, N.N.T.; Dao, A.T.N.; Kato, K.; Ikenaga, T.; Trinh, D.X.; Taniike, T. One-pot synthesis of TiO₂/graphene nanocomposites for excellent visible light photocatalysis based on chemical exfoliation method. *Carbon* **2018**, *133*, 109–117. [[CrossRef](#)]
9. Luo, H.; Dimitrov, S.; Daboczi, M.; Kim, J.S.; Guo, Q.; Fang, Y.; Stoeckel, M.A.; Samori, P.; Fenwick, O.; Sobrido, A.B.J.; et al. Nitrogen-Doped Carbon Dots/TiO₂ Nanoparticle Composites for Photoelectrochemical Water Oxidation. *ACS Appl. Nano Mater.* **2020**, *3*, 3371–3381. [[CrossRef](#)]
10. Wang, H.; Lu, J.; Liu, L.; Cui, W.; Liang, Y. Ultra-thin rGO nanosheet modified TiO₂ nanotube arrays for boosted photoelectrochemical performance. *Appl. Surf. Sci.* **2020**, *506*, 144966. [[CrossRef](#)]
11. Chen, S.; Zhou, Y.; Luo, H.; Tang, L.; Guo, R.; Zhang, D. Core-shell TiO₂@HfO₂ nanowire arrays with designable shell thicknesses for improved permittivity and energy density in polymer nanocomposites. *Compos. Part A Appl. Sci. Manuf.* **2020**, *137*, 1060122. [[CrossRef](#)]
12. Zhao, T.; Qian, R.; Tang, Y.; Yang, J.; Dai, Y.; Lee, W.I.; Pan, J.H. Controllable Synthesis and Crystallization of Nanoporous TiO₂ Deep-Submicrospheres and Nanospheres via an Organic Acid-Mediated Sol–Gel Process. *Langmuir* **2020**, *36*, 7447–7455. [[CrossRef](#)]
13. Yang, T.; Shin, D.S.; Yu, J.; Ji, Y.; Kim, T.G.; Dayakar, T.; Park, J. Fabrication of n-TiO₂ hollow spheres monolayer-based UV detectors with different-sized nanospheres. *Semicond. Sci. Technol.* **2018**, *33*, 125018. [[CrossRef](#)]
14. Dong, G.; Xia, D.; Yang, Y.; Zhang, W.; Fan, R.; Sui, L.; Su, L.; Zhao, Y.; Yang, P.; Li, Y. In-situ passivation of TiO₂ mesoporous scaffold with nano-sized heteropolyacid for boosting the efficiency of the perovskite solar cells. *Electrochim. Acta* **2020**, *332*, 135427. [[CrossRef](#)]
15. Leem, Y.C.; Seo, O.; Jo, Y.R.; Kim, J.H.; Chun, J.; Kim, B.J.; Noh, D.Y.; Lim, W.; Kim, Y.; Park, S.J. Titanium oxide nanotube arrays for high light extraction efficiency of GaN-based vertical light-emitting diodes. *Nanoscale* **2016**, *8*, 10138–10144. [[CrossRef](#)]
16. Désières, Y.; Chen, D.Y.; Visser, D.; Schippers, C.; Anand, S. Strong light extraction enhancement using TiO₂ nanoparticles-based microcone arrays embossed on III-Nitride light emitting diodes. *Appl. Phys. Lett.* **2018**, *112*, 231101. [[CrossRef](#)]
17. Celik, E.; Negi, R.S.; Bastianello, M.; Boll, D.; Mazilkin, A.; Brezesinski, T.; Elm, M.T. Tailoring the protonic conductivity of porous yttria-stabilized zirconia thin films by surface modification. *Phys. Chem. Chem. Phys.* **2020**, *22*, 1519–1528. [[CrossRef](#)]
18. Kenanakis, G.; Katsarakis, N. Chemically grown TiO₂ on glass with superior photocatalytic properties. *J. Environ. Chem. Eng.* **2014**, *2*, 1748–1755. [[CrossRef](#)]
19. Démarest, N.; Deubel, D.; Keromnès, J.C.; Vaudry, C.; Grasset, F.; Lefort, R.; Guilloux-Viry, M. Optimization of bandpass optical filters based on TiO₂ nanolayers. *Opt. Eng.* **2015**, *54*, 015101. [[CrossRef](#)]
20. Kim, T.G.; Park, S.J.; Kim, D.; Shin, D.S.; Park, J. Improvement of the Optical and Electrical Performance of GaN-Based Light-Emitting Diodes (LEDs) Using Transferrable ZnSnO₃ (ZTO) Microsphere Monolayers. *ACS Sustain. Chem. Eng.* **2018**, *6*, 11547–11554. [[CrossRef](#)]

21. Shin, D.S.; Kim, T.G.; Kim, D.; Kim, K.K.; Park, J. Light Extraction Enhancement of GaN-Based Light-Emitting Diodes Using Hollow Silica Nanospheres. *J. Nanosci. Nanotech.* **2017**, *17*, 4073–4077. [[CrossRef](#)]
22. Jung, U.; Kim, S.; Kim, D.; Shin, D.S.; Xian, Z.; Park, J. Metal—Semiconductor—Metal UV Detectors Using Transferrable Amorphous and Crystalline Zinc-Tin-Oxide Microsphere Monolayers. *ACS Sustainable Chem. Eng.* **2020**, *8*, 60–70. [[CrossRef](#)]
23. Lu, Z.; Hanif, A.; Lu, C.; Sun, G.; Cheng, Y.; Li, Z. Thermal, mechanical, and surface properties of poly(vinyl alcohol) (PVA) polymer modified cementitious composites for sustainable development. *J. Appl. Polym. Sci.* **2018**, *1*, 46177. [[CrossRef](#)]
24. Kim, D.; Song, K.M.; Jung, U.; Kim, S.; Shin, D.S.; Park, J. Effects of Different InGaN/GaN Electron Emission Layers/Interlayers on Performance of a UV-A LED. *Appl. Sci.* **2020**, *10*, 1514. [[CrossRef](#)]
25. Ji, Y.; Jung, U.; Xian, Z.; Kim, D.; Yu, J.; Park, J. Ultraviolet photodetectors using hollow p-CuO nanospheres/n-ZnO nanorods with a pn junction structure. *Sens. Actuator A Phys.* **2020**, *304*, 111876. [[CrossRef](#)]
26. Wei, Y.; Zhu, J.; Gan, Y.; Cheng, G. Titanium glycolate-derived TiO₂ nanomaterials: Synthesis and applications. *Adv. Powder Technol.* **2018**, *29*, 2289–2311. [[CrossRef](#)]
27. Zhao, T.; Qian, R.; Zhou, G.; Wang, Y.; Lee, W.I.; Pan, J.H. Mesoporous WO₃/TiO₂ spheres with tailored surface properties for concurrent solar photocatalysis and membrane filtration. *Chemosphere* **2021**, *263*, 128344. [[CrossRef](#)]
28. Karimi Estahbanati, M.R.; Feilizadeh, M.; Shokrollahi Yancheshmeh, M.; Iliuta, M.C. Effects of Carbon Nanotube and Carbon Sphere Templates in TiO₂ Composites for Photocatalytic Hydrogen Production. *Ind. Eng. Chem. Res.* **2019**, *58*, 2770–2783. [[CrossRef](#)]
29. Su, D.; Dou, S.; Wang, G. Anatase TiO₂: Better Anode Material Than Amorphous and Rutile Phases of TiO₂ for Na-Ion Batteries. *Chem. Mater.* **2015**, *27*, 6022–6029. [[CrossRef](#)]
30. Alamelu, K.; Ali, B.J. Sunlight driven photocatalytic performance of a Pt nanoparticle decorated sulfonated graphene–TiO₂ nanocomposite. *New J. Chem.* **2020**, *44*, 7501–7516. [[CrossRef](#)]
31. Scirè, D.; Macaluso, R.; Mosca, M.; Casaletto, M.P.; Isabella, O.; Zeman, M.; Crupi, I. Density of states characterization of TiO₂ films deposited by pulsed laser deposition for heterojunction solar cells. *Nano Res.* **2022**, *5*, 4048–4057. [[CrossRef](#)]
32. Leung, S.F.; Zhang, Q.; Xiu, F.; Yu, D.; Ho, J.C.; Li, D.; Fan, Z. Light Management with Nanostructures for Optoelectronic Devices. *J. Phys. Chem. Lett.* **2014**, *5*, 1479–1495. [[CrossRef](#)] [[PubMed](#)]
33. Al-Amri, A.M.; Fu, P.H.; Lai, K.Y.; Wang, H.P.; Li, L.J.; He, J.H. Efficiency Enhancement of InGaN-Based Solar Cells via Stacking Layers of Light-Harvesting Nanospheres. *Sci. Rep.* **2016**, *6*, 28671. [[CrossRef](#)] [[PubMed](#)]

Disclaimer/Publisher’s Note: The statements, opinions and data contained in all publications are solely those of the individual author(s) and contributor(s) and not of MDPI and/or the editor(s). MDPI and/or the editor(s) disclaim responsibility for any injury to people or property resulting from any ideas, methods, instructions or products referred to in the content.